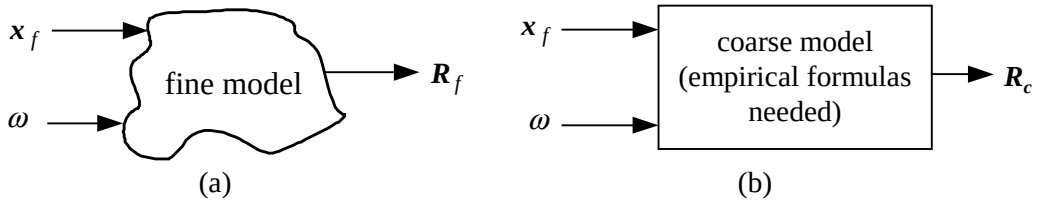

Fig. 1. The fine model (a) and the coarse model (b).

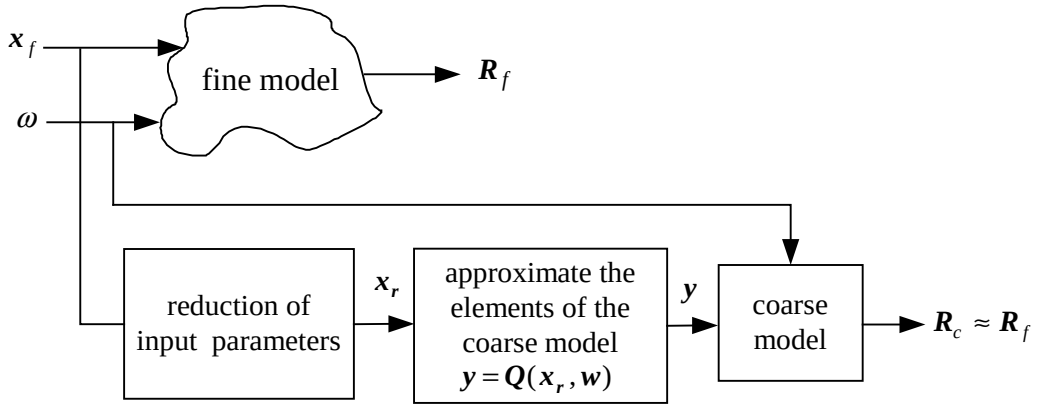

Fig. 2. The development of the frequency-independent empirical model (FIEM).

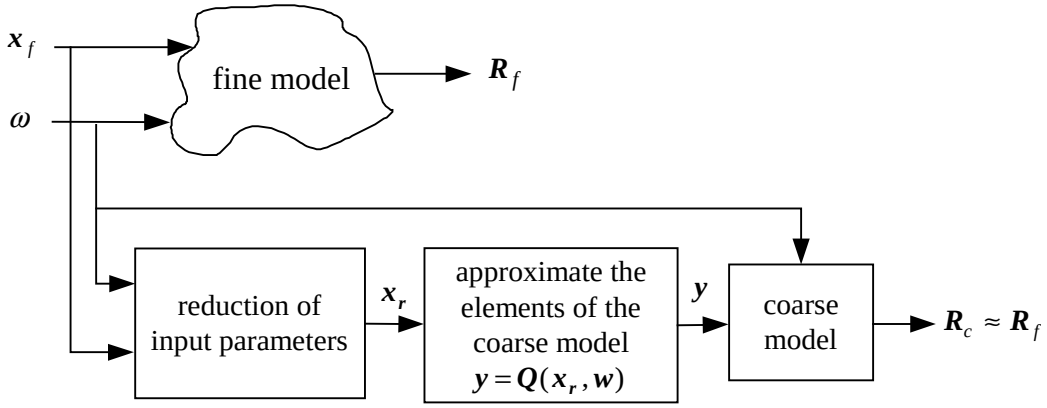

Fig. 3. The development of the FDEM with elements explicitly function of frequency.

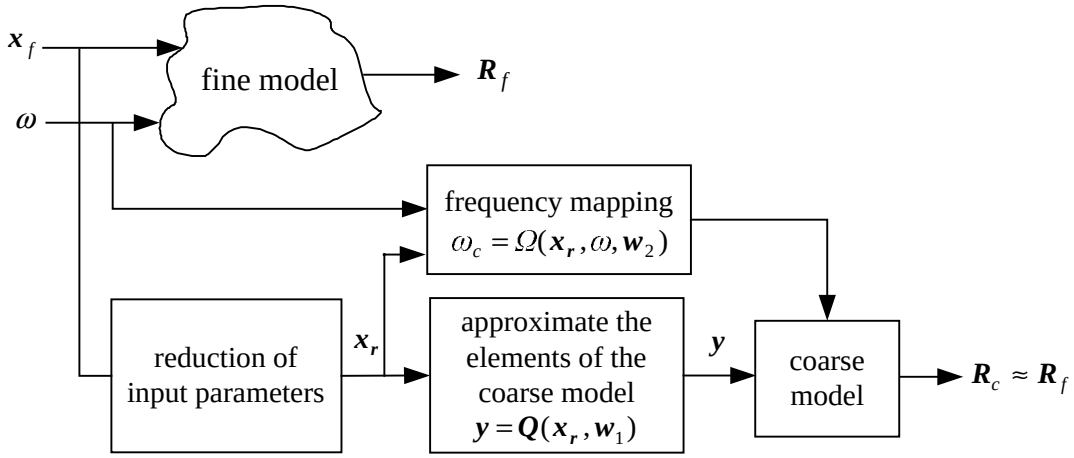

Fig. 4. The development of the FDEM with elements implicitly function of frequency through frequency mapping.

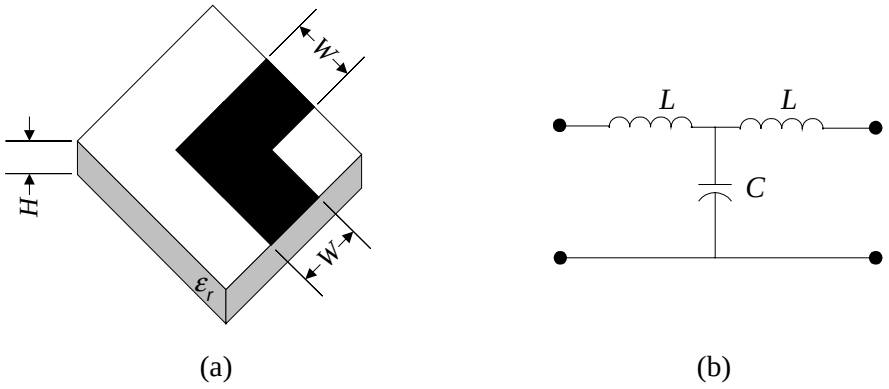

Fig. 5. The microstrip right angle bend: (a) the fine model, (b) the coarse model.

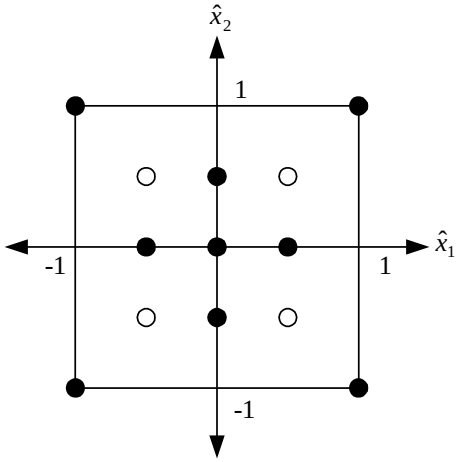

Fig. 6. The training points for the microstrip right angle bend.

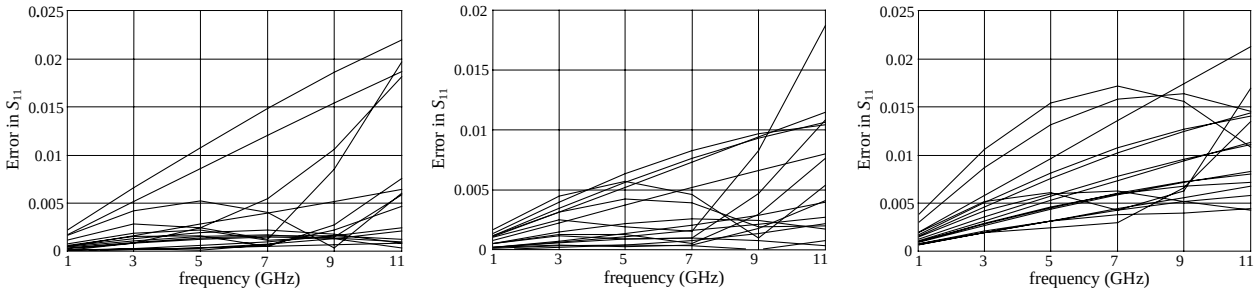

Fig. 7. The error in S_{11} of the microstrip right angle bend with respect to ***em***^{TM} at the test points: (a) the FIEM developed by ANNs, (b) the FIEM developed by MRFs, (c) by the empirical model in [14].

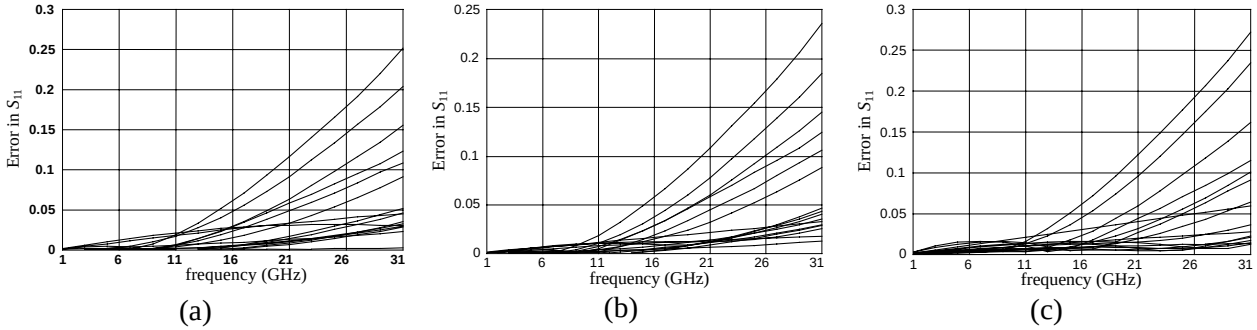

Fig. 8. The error in S_{11} of the microstrip right angle bend with respect to ***em***^{TM} over a broad frequency range: (a) the FIEM developed by ANNs, (b) the FIEM developed by MRFs, (c) the empirical model in [14].

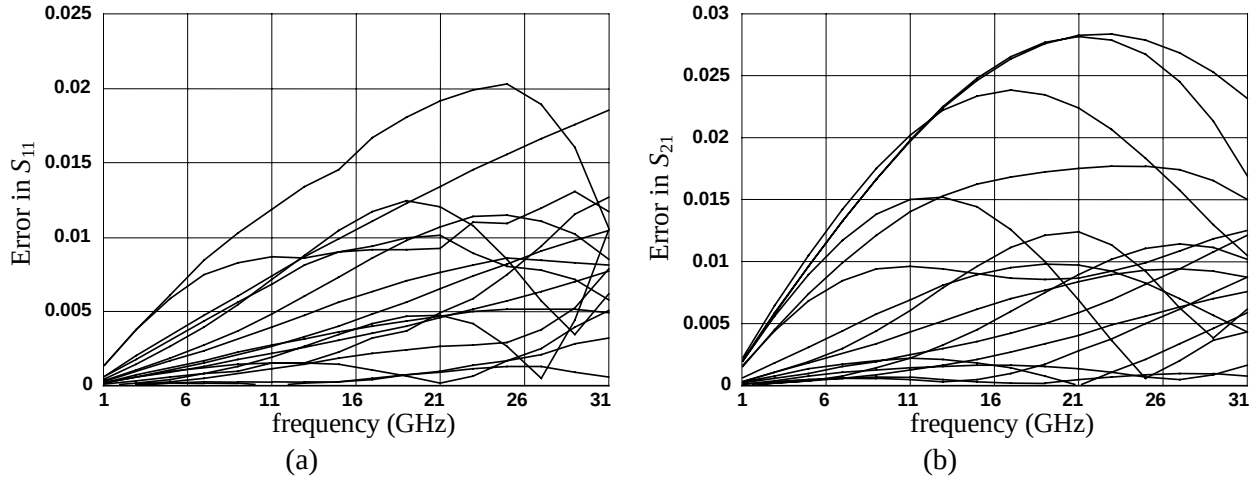

Fig. 9. Error of the FDEM of the microstrip right angle bend (developed by MRFs) with respect to ***em***^{TM} at the test points: (a) in S_{11}, (b) in S_{21}.

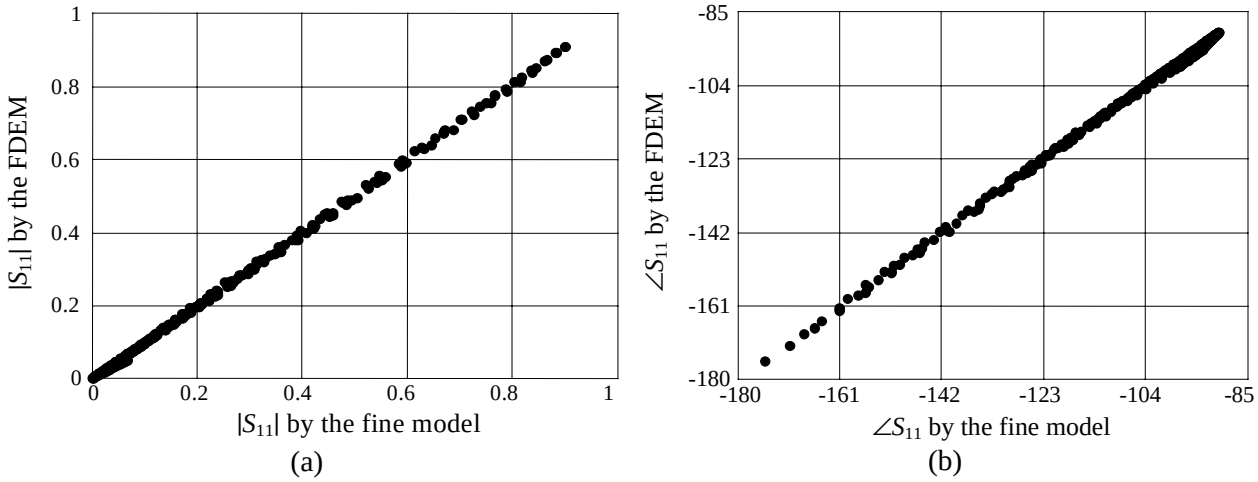

Fig. 10. Comparison between the responses obtained by the FDEM of the microstrip right angle bend and those obtained by ***em***™ at the test points: (a) magnitude of S_{11}, (b) phase of S_{11} in degrees.

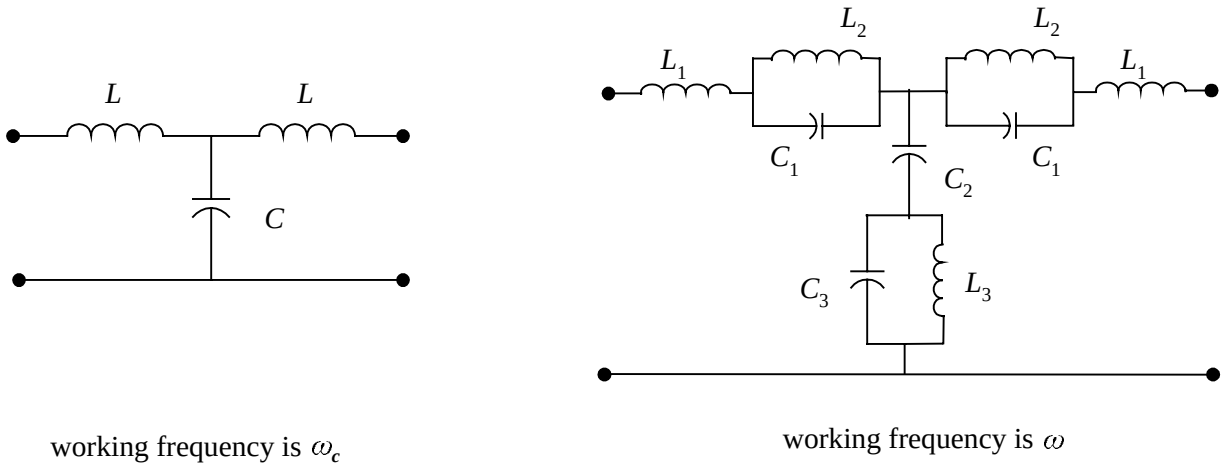

Fig. 11. The FDEM of the microstrip right angle bend (a) and the equivalent FIEM (b).

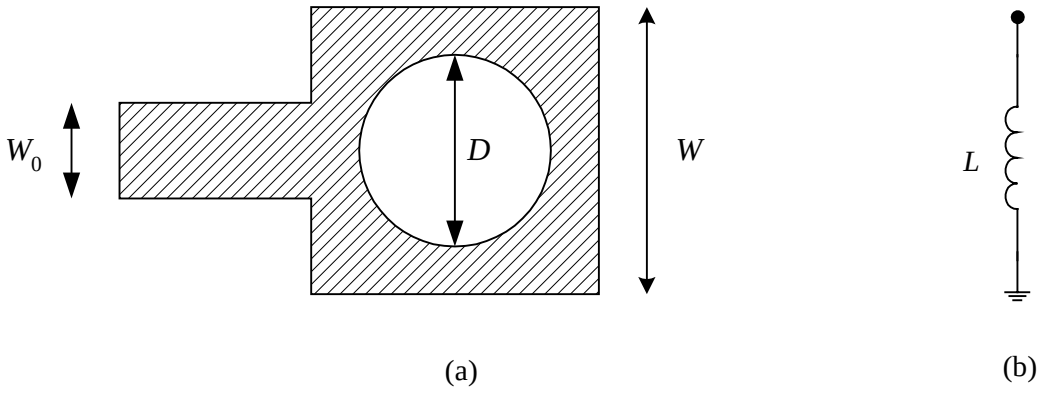

Fig. 12. The microstrip via: (a) the physical structure, (b) the coarse model (equivalent circuit).

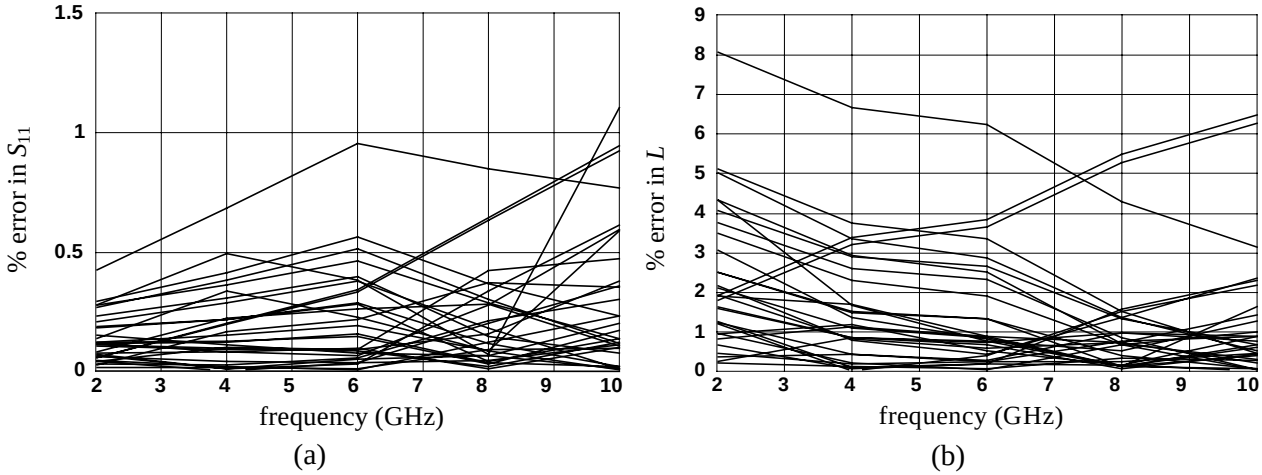

Fig. 13. Percentage error of the FIEM of the microstrip via with respect to ***em***™ at the test points: (a) in S_{11}, (b) in L.

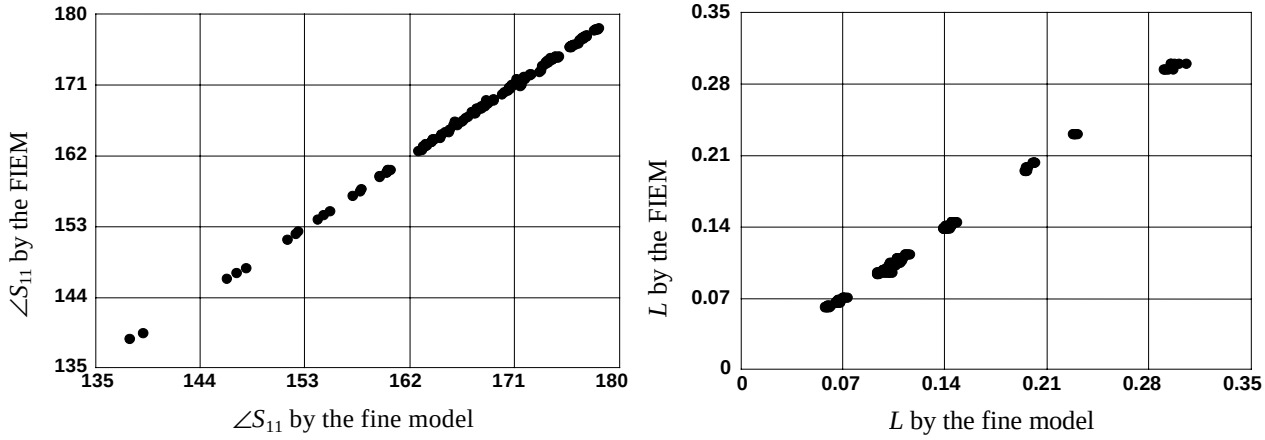

Fig. 14. Comparison between the responses obtained by the FIEM of the microstrip via and those obtained by ***em***™ at the test points in the frequency range [2, 10] GHz: (a) phase of S_{11}, (b) the inductance L.

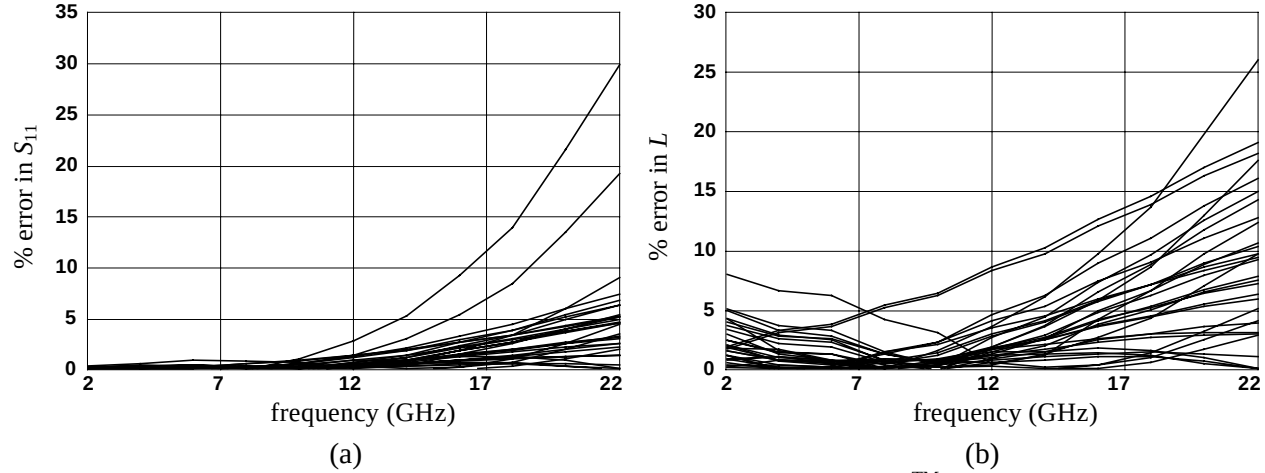

Fig. 15. Comparison of the FIEM of the microstrip via with respect to ***em***™ over a broad frequency range at the test points: (a) % error in S_{11}, (b) % error in L.

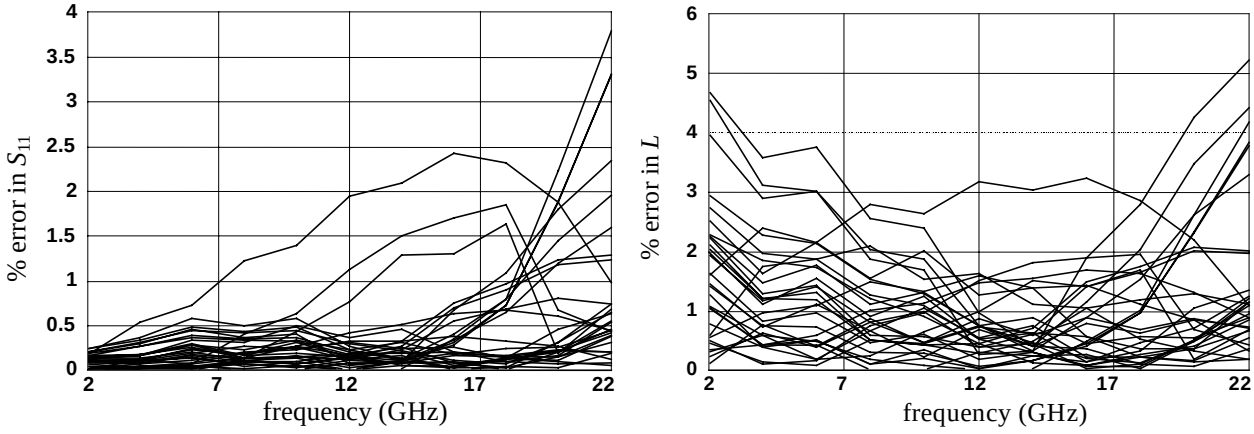

(a) (b)

Fig. 16. Comparison of the FDEM of the microstrip via with respect to ***em***™ over a broad frequency range at the test points: (a) % error in S_{11}, (b) % error in L.

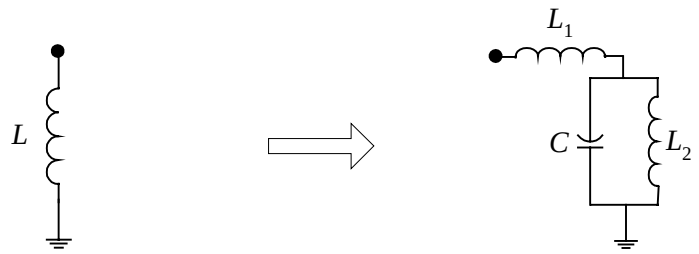

working frequency is ω_c working frequency is ω

(a) (b)

Fig. 17. The FDEM of the microstrip via (a) and the corresponding FIEM (b).

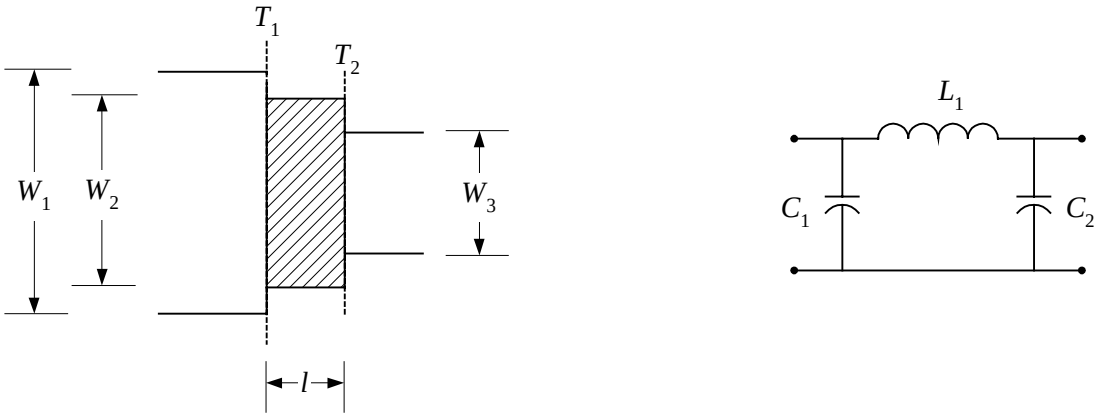

(a) (b)

Fig. 18. The microstrip double-step: (a) the physical structure where T_1 and T_2 are the reference planes, (b) the coarse model.

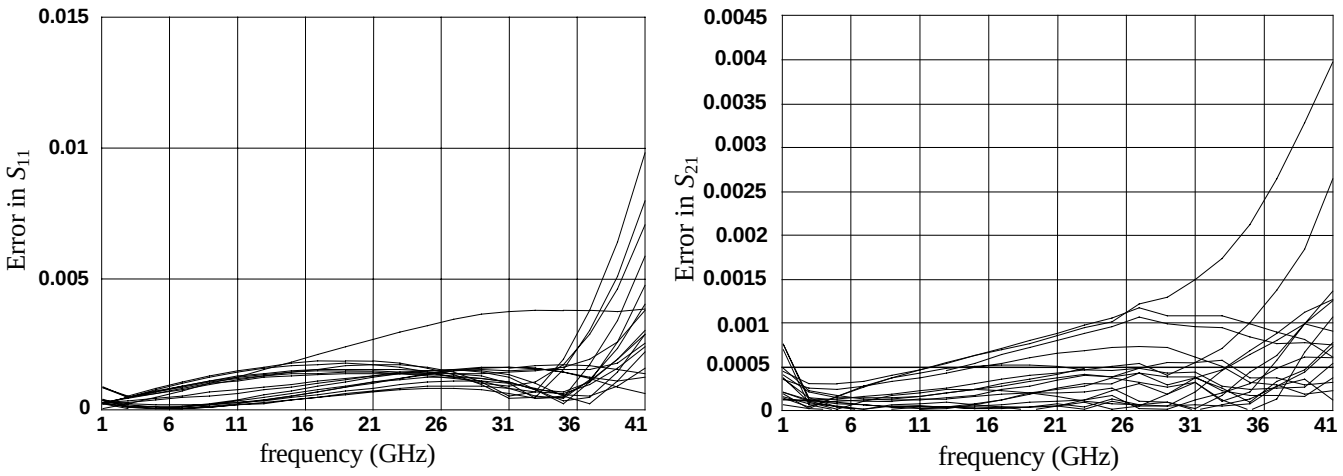

Fig. 19. Comparison between the FDEM of the double-step element and ***em***™ at the test points in the region of interest: (a) error in S_{11}, (b) error in S_{21}.

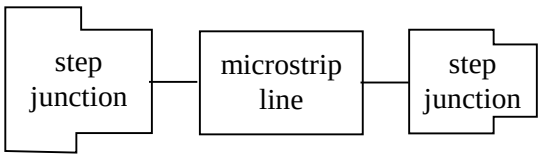

Fig. 20. An alternative model for the microstrip double-step element.

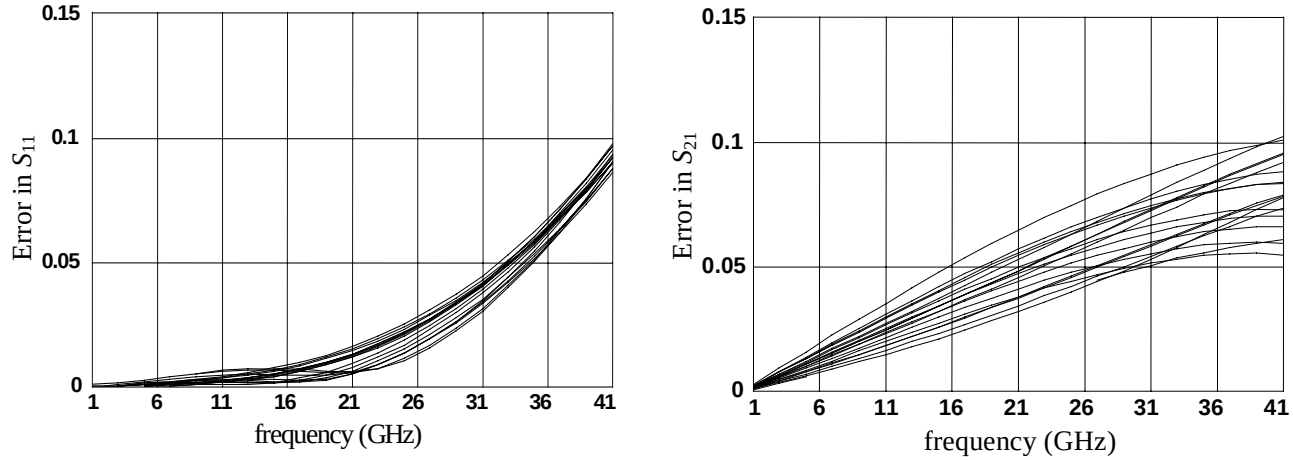

Fig. 21. Comparison between the double-step model in Fig.20 and ***em***™ at the test points in the region of interest: (a) error in S_{11}, (b) error in S_{21}.

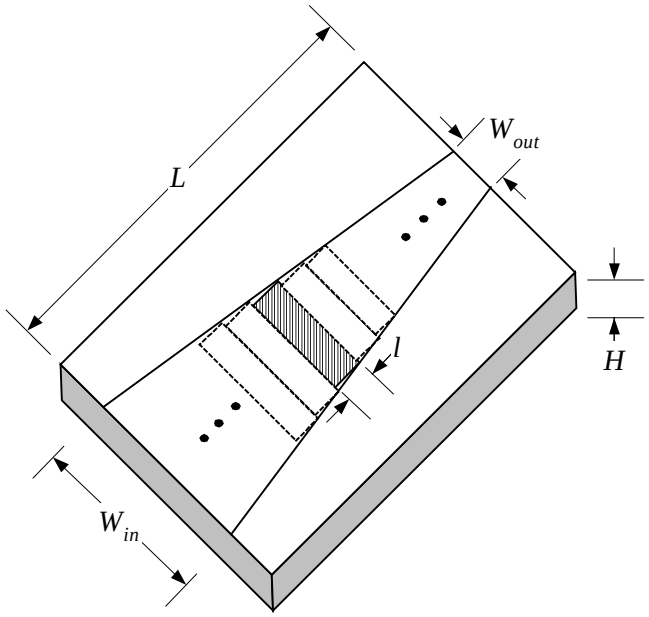

Fig. 22. Linear tapered microstrip line.

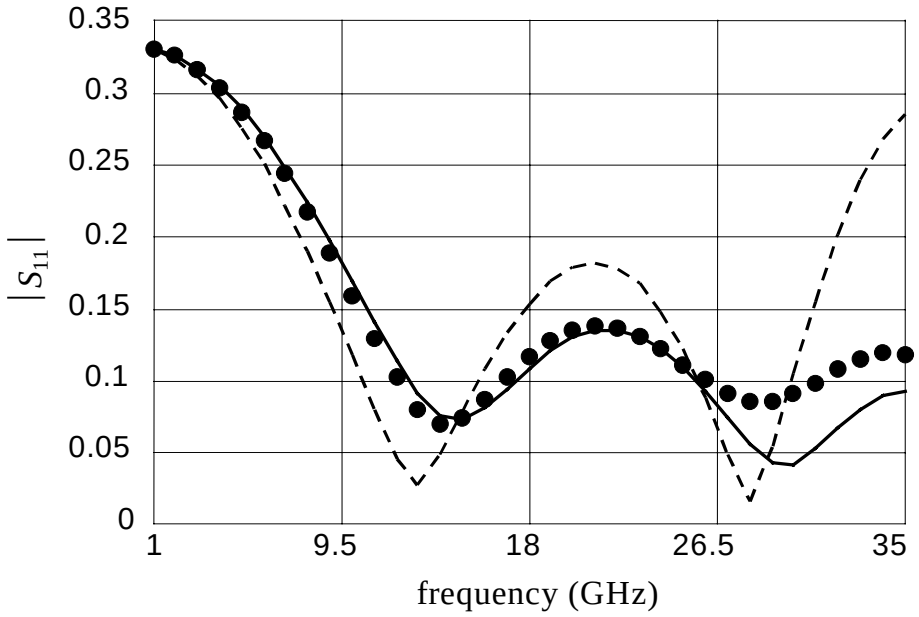

Fig. 23. The response of the linear tapered microstrip line by ***em***™ (• •), by the FDEM of the double-step element (—), by the model in Fig.20 of the double-step element (----).

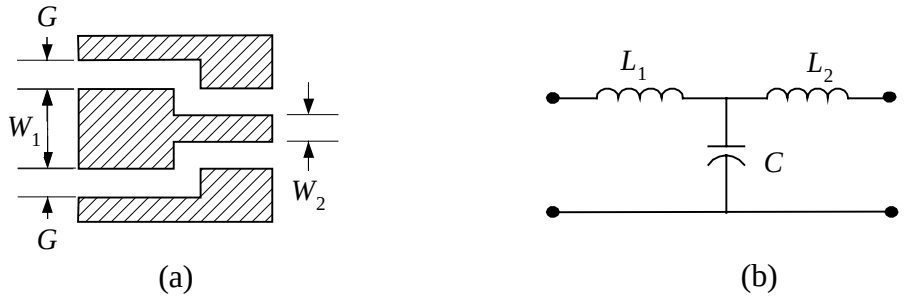

Fig. 24. The CPW step junction: (a) the physical structure, (b) the coarse model.

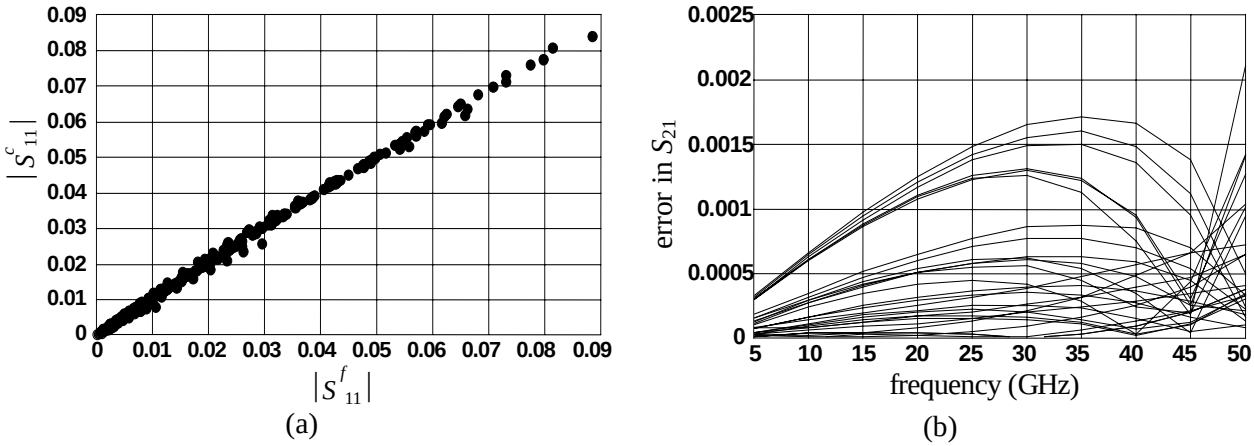

Fig. 25. Comparison between the results obtained by ***em***™ and by the FIEM of the CPW step junction: (a) $|S_{11}|$ by ***em***™ versus that of the FIEM, (b) the error in S_{21}.

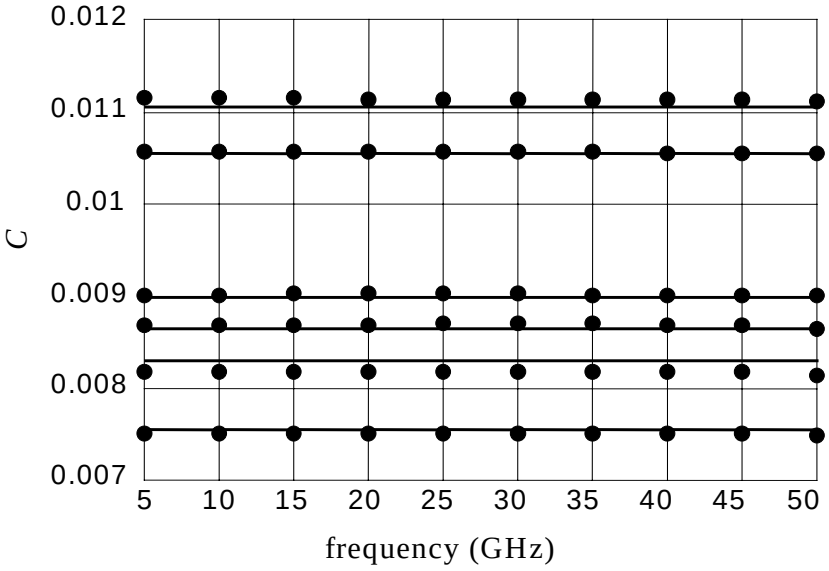

Fig. 26. The capacitance of the CPW step junction: (a)extracted from the fine model (• •), (b) predicted by the FIEM of the CPW step junction (—).